Simultaneous Hydrolysis and Detection of Organophosphate by Benzimidazole Containing Ligand-Based Zinc(II) Complexes

Gaber Mersal, Hamdy El-Sheshtawy, Mohammed Amin, Nasser Mostafa, Amine Mezni, Sarah Alharthi, Rabah Boukherroub, Mohamed Ibrahim

▶ **To cite this version:**

Gaber Mersal, Hamdy El-Sheshtawy, Mohammed Amin, Nasser Mostafa, Amine Mezni, et al.. Simultaneous Hydrolysis and Detection of Organophosphate by Benzimidazole Containing Ligand-Based Zinc(II) Complexes. Crystals, 2021, 11 (6), pp.714. 10.3390/cryst11060714 . hal-03442205

HAL Id: hal-03442205
https://hal.science/hal-03442205v1

Submitted on 30 May 2022

HAL is a multi-disciplinary open access archive for the deposit and dissemination of scientific research documents, whether they are published or not. The documents may come from teaching and research institutions in France or abroad, or from public or private research centers.

L'archive ouverte pluridisciplinaire **HAL**, est destinée au dépôt et à la diffusion de documents scientifiques de niveau recherche, publiés ou non, émanant des établissements d'enseignement et de recherche français ou étrangers, des laboratoires publics ou privés.

Distributed under a Creative Commons Attribution 4.0 International License

crystals

MDPI

Article

Simultaneous Hydrolysis and Detection of Organophosphate by Benzimidazole Containing Ligand-Based Zinc(II) Complexes

Gaber A. M. Mersal [1,*], Hamdy S. El-Sheshtawy [2], Mohammed A. Amin [1], Nasser Y. Mostafa [3], Amine Mezni [1], Sarah Alharthi [1], Rabah Boukherroub [4] and Mohamed M. Ibrahim [1,*]

[1] Chemistry Department, Faculty of Science, Taif University, Al Hawiyah, Taif 26571, Saudi Arabia; mohamed@tu.edu.sa (M.A.A.); aminemrezni@yahoo.fr (A.M.); world-sososo-2007@hotmail.com (S.A.)
[2] Chemistry Department, Faculty of Science, Kafrelsheikh University, Kafr El-Sheikh 33516, Egypt; h.elsheshtawy@sci.kfs.edu.eg
[3] Chemistry Department, Faculty of Science, Suez Canal University, Ismailia Governorate 41522, Egypt; nmostafa@yahoo.com
[4] University of Lille, CNRS, Centrale Lille, ISEN, University of Valenciennes, UMR 8520—IEMN, 59000 Lille, France; rabah.boukheroub@univ-lille.fr
* Correspondence: gamersal@ytu.edu.sa (G.A.M.M.); ibrahim@tu.edu.sa (M.M.I.)

Abstract: The agricultural use of organophosphorus pesticides is a widespread practice with significant advantages in crop health and product yield. An undesirable consequence is the contamination of soil and groundwater by these neurotoxins resulting from over application and run-off. Here, we design and synthesize the mononuclear zinc(II) complexes, namely, $[Zn(AMB)_2Cl](ClO_4)$ **1** and $[Zn(AMB)_2(OH)](ClO_4)$ **2** (AMB = 2-aminomethylbenzimidazole), as artificial catalysts inspired by *phosphotriesterase* (PTE) for the hydrolysis of organophosphorus compounds (OPs) and simultaneously detect the organophosphate pesticides such as fenitrothion and parathion. Spectral and DFT (B3LYP/Lanl2DZ) calculations revealed that complexes **1** and **2** have a square-pyramidal environment around zinc(II) centers with coordination chromophores of ZnN_4Cl and ZnN_4O, respectively. Both **1** and **2** were used as a modifier in the construction of a biomimetic sensor for the determination of toxic OPs, fenitrothion and parathion, in phosphate buffer by square wave voltammetry. The hydrolysis of OPs using **1** or **2** generates *p*-nitrophenol, which is subsequently oxidized at the surface of the modified carbon past electrode. The catalytic activity of **2** was higher than **1**, which is attributed to the higher electronegativity of the former. The oxidation peak potentials of *p*-nitrophenol were obtained at +0.97 V (vs. Ag/AgCl) using cyclic voltammetry (CV) and +0.88 V (vs. Ag/AgCl) using square wave voltammetry. Several parameters were investigated to evaluate the performance of the biomimetic sensor obtained after the incorporation of zinc(II) complex **1** and **2** on a carbon paste electrode (CPE). The calibration curve showed a linear response ranging between 1.0 µM (0.29 ppm) and 5.5 µM (1.6 ppm) for fenitrothion and 1.0 µM (0.28 ppm) and 0.1 µM (0.028 ppm) for parathion with a limit of detection (LOD) of 0.08 µM (0.022 ppm) and 0.51 µM (0.149 ppm) for fenitrothion and parathion, respectively. The obtained results clearly demonstrated that the CPE modified by **1** and **2** has a remarkable electrocatalytic activity towards the hydrolysis of OPs under optimal conditions.

Keywords: benzimidazole containing Zn(II) ligand; biomimetic; organophosphate hydrolysis; carbon paste electrode; electrochemical detection; fenitrothion; parathion

check for updates

Citation: Mersal, G.A.M.; El-Sheshtawy, H.S.; Amin, M.A.; Mostafa, N.Y.; Mezni, A.; Alharthi, S.; Boukherroub, R.; Ibrahim, M.M. Simultaneous Hydrolysis and Detection of Organophosphate by Benzimidazole Containing Ligand-Based Zinc(II) Complexes. *Crystals* **2021**, *11*, 714. https://doi.org/10.3390/cryst11060714

Academic Editor: Paola Paoli

Received: 30 March 2021
Accepted: 7 June 2021
Published: 21 June 2021

Publisher's Note: MDPI stays neutral with regard to jurisdictional claims in published maps and institutional affiliations.

Copyright: © 2021 by the authors. Licensee MDPI, Basel, Switzerland. This article is an open access article distributed under the terms and conditions of the Creative Commons Attribution (CC BY) license (https://creativecommons.org/licenses/by/4.0/).

1. Introduction

The development of zinc(II) complexes as biomimetic systems for *metallophosphatase* enzymes as well as potential catalysts for the detoxification of organophosphate (OPs) esters is of a fundamental interest since these compounds appear from day-to-day applications such as pesticides [1–4]. The harmful effects of OPs are related to their inhibition of mammalian *acetylcholinesterase*, an enzyme responsible for regulating the in vivo concentration of the neuro-transmitter acetylcholine [5]. Therefore, the fast decomposition of toxic

OPs compounds to non-toxic molecules is useful from the view of environmental protection. In addition, determination of the OPs hydrolysis by-products such as *p*-nitrophenolate in these environmental samples is very important due to its higher toxicity.

Enzyme-based biosensors are widely used for OPs quantification [6–8]. However, enzyme stability, specific activity and significant inhibition of the immobilized enzyme caused by the reaction products can influence the response of such type of biosensors. Additionally, biosensors are not robust and their lifetimes are limited by denaturation of biological materials present on the electrode surface [9]. To overcome these disadvantages, a new alternative method is based on mimicking the active site of hydrolytic enzymes [10–12]. For example, the reduction approach was used to model the essential features of the active site [13]. Although these primitive synthetic models are far different from enzymes, they can contribute in gaining insight into the enzyme mechanism and its important structural features [14,15]. Furthermore, such mechanistic insight can lead to development of new catalysts for various transformations [16]. The use of benzimidazole-containing ligands was successfully utilized for the preparation and isolation of different structural zinc(II) enzyme model complexes [17,18] and was also suitable for the synthesis of biomimetic coordination compounds having *carbonic anhydrase* and *phosphatase* activity [18,19]. These ligands were designed to coordinate to the zinc(II) ion while leaving zinc(II) coordinatively unsaturated, enabling the coordination of a water molecule. The aqua zinc complexes $[(L)Zn(OH_2)]^{2+}$ formed can then generate $[(L)Zn(OH)]^{+}$ species at the catalytic site during the hydrolytic action of zinc enzyme model complexes [1–3].

Many analytical methods have been developed for the highly sensitive, selective, rapid and reliable detection of OPs compounds. These methods include high-performance liquid chromatography with diode-array detection [20], liquid chromatography–mass spectrometry [21], gas chromatography and liquid chromatography [22]. However, these methods are time-consuming and require expensive equipment. On the other hand, electroanalytical methods offer several advantages such as low cost, speed of analysis, higher selectivity and sensitivity as well as easy operation and lower detection limit [23,24]. Electrochemical techniques through modifying electrodes with active catalysts have been employed for the determination of organophosphate [25–28]. For example, electrodes modified with different nanocomposite such as CuO-TiO_2 [29], Ag/graphene [30], Au/MWCNT [31], ZrO_2/Au [32], ZnO/GO [33], Zr(IV)/Au [34] and MnO_2 [35] have been used for the detection of organophosphate compounds. However, to the best of our knowledge, there is no data reported for metal complexes modified carbon-based electrodes for both hydrolysis and sensing applications.

In this work, a biomimetic sensor was prepared through modification of a carbon paste electrode with zinc(II) complex $[Zn(AMB)_2Cl](ClO_4)$ **1**, and $[Zn(AMB)_2(OH)](ClO_4)$ **2,** derived from the bidentate ligand 2-aminomethylbenzimidazole dihydrochloride (AMB·2HCl) as a structural and functional mimic for the active site of *hydrolase* enzyme. The electrochemical behavior of the prepared biomimetic sensor was assessed using cyclic voltammetry (CV) and electrochemical impedance spectroscopy (EIS) techniques. The electrochemical behaviors of fenitrothion and parathion on the obtained biomimetic sensor were studied by cyclic and square wave voltammetric techniques. The effects of different experimental parameters such as supporting electrolyte, pH, deposition potential, accumulation time and different square wave voltammetric parameters on the peak height have also been investigated.

2. Experimental

2.1. Materials and Instrumentations

The ligand 2-aminomethylbenzimidazole dihydrochloride (AMB·2HCl), graphite powder, paraffin wax, fenitrothion and parathion were obtained from Sigma-Aldrich. Zinc(II) complex **1** was previously obtained [36]. Infrared spectral measurements of the free ligand and its zinc complexes **1** and **2** were recorded using Alpha-Attenuated FT-IR Spectrophotometer, Bruker, in the range of 400–4000 cm^{-1}. Raman spectra were recorded on a Bruker

FT-Raman at room temperature with a germanium detector, maintained at liquid nitrogen temperature using 1064.0 nm radiation, generated by a Nd–YAG laser with a resolution of 2 cm^{-1}. ^1H NMR spectra were obtained using Varian 400-NMR spectrophotometer employing TMS as a reference and DMSO-d_6 as a solvent at ambient temperature. The specific conductance of the complexes was measured using freshly prepared (10^{-3} M) solutions in water at ambient temperature, using YSI Model 32 conductance meter. Cyclic voltammetry (CV) and square wave voltammetry were performed using an Autolab potentiostat PGSTAT 302 (Eco Chemie, Utrecht, The Netherlands) driven by the General Purpose Electrochemical Systems data processing software (GPES, software version 4.9, Eco Chemie). Electrochemical cell with three electrodes was used; unmodified carbon paste electrode or carbon paste electrode modified zinc(II) complex **1** was used as a working electrode, Ag/AgCl was used as a reference electrode, while platinum wire was used as a counter electrode. The pH values were measured using a Metrohom pH-meter with a combined glass electrode. The pH values were adjusted using 1 M NaOH aqueous solution.

2.2. Synthesis of Zinc(II) Complex [(AMB)$_2$Zn-OH]ClO$_4$ **2**

A solution of zinc(II) complex **1** (0.494 g, 1.0 mM) in methanol (5 mL) was treated with a solution of NaOH (40 mg, 1.0 mM) in methanol (5 mL). The resulting solution was stirred for additional 2 h. The solution was concentrated to 5 mL. Colorless crystals were obtained after several days, separated through filtration and dried in vacuum. Anal. Calcd. for $C_{16}H_{19}ClN_6O_5Zn$ (476.2): C, 40.36; H, 4.02; N, 17.65; Cl, 7.45; Zn, 13.73%. Found: C, 39.98; H, 3.79; N, 17.87; Cl, 7.67; Zn, 13.55%. ^1H NMR (400 MHz; CD_3OD:D_2O): 4.03 (4H, s, –CH_2–), 7.11, (4H, H_b) and 7.13 (4H, H_a).

2.3. Preparation of CPE and Modified CPE by Zinc(II) Complex ***1*** *and* ***2***

Unmodified CPE was prepared by hand mixing graphite powder 65% with hot paraffin wax 35% to produce a homogeneous paste. The obtained carbon paste was packed into the end of a syringe (2 mm). An external electrical contact was established by forcing a copper wire down the syringe. Modified CPE by Zn(II) complex **1** and **2** were prepared by mixing 60% of graphite powder and 30% of paraffin wax with 10% of zinc(II) complex **1** or complex **2**. The surface of the electrode was polished with a piece of weighing paper and then rinsed with distilled water.

2.4. DFT Calculations

Theoretical calculations were performed using Gaussian09 program [37]. All molecular complexes were optimized at B3LYP/6-311G+(d,*p*) level of theory for H, C, N and Cl, and B3LYP/Lanl2DZ for Zn atom. Analytical frequency calculations were done in order to verify the stationary points on the potential energy surface. Time-dependent density functional theory (TD−DFT) was conducted at the optimized structures in order to calculate the HUMO and LUMO orbital energies.

3. Results and Discussion

3.1. Structure Optimization and Characterization of Complexes ***1*** *and* ***2***

The reaction of $Zn(ClO_4)_2{\cdot}H_2O$ with two molar amounts of the ligand, 2-aminomethylbenzimidazole dihydrochloride (AMB·2HCl), treated with NaOH in methanol leads to the formation of the ionic compound $[Zn(AMB)_2Cl]ClO_4$ **1**. Subsequent addition of an equimolar amount of NaOH to zinc(II) complex **1** in methanol yields the hydroxo complex $[Zn(AMB)_2(OH)]ClO_4$ **2**. Although complex **2** was stable in the solution, attempts to obtain the single crystal failed. The molecular structure of complex **1** with 50% probability thermal ellipsoids is depicted in Figure 1a [36]. The complex consists of one discrete pseudo-square pyramidal $[Zn(AMB)_2Cl]^+$ cation and one ClO_4^- anion. DFT optimized structure at B3LYP/Lanl2DZ level of **1** shows an agreement for both the bond length and bond angles, taking into account effect of solvent and counter ion. The 2D structure of complex **1** shows an endless network stabilized by

strong hydrogen bonding (HB) (Figure 1c). Strong HB was formed between the bonded Cl atom and H (d = 2.51 Å and C-Cl ... H = 127°). The HB bond length and bond angles are in accordance with similar strong HB [36]. The uncoordinated oxygen atom of perchlorate ion accepts the protons from the ligand to connect the network in the a-direction. Figure 1b shows the optimized structure (B3LYP/Lanl2DZ) of the analogue complex **2**. The Zn1 ... O-H bond was 1.93 Å, which is lower than the corresponding Zn1 ... Cl bond, which is attributed to the more electronegativity of O atom and similar to literature values [38]. Similar to complex **1**, the bond length of the Zn1 ... N(1,4) primary amine was longer than the Zn1 ... N(2,5) in heterocyclic system.

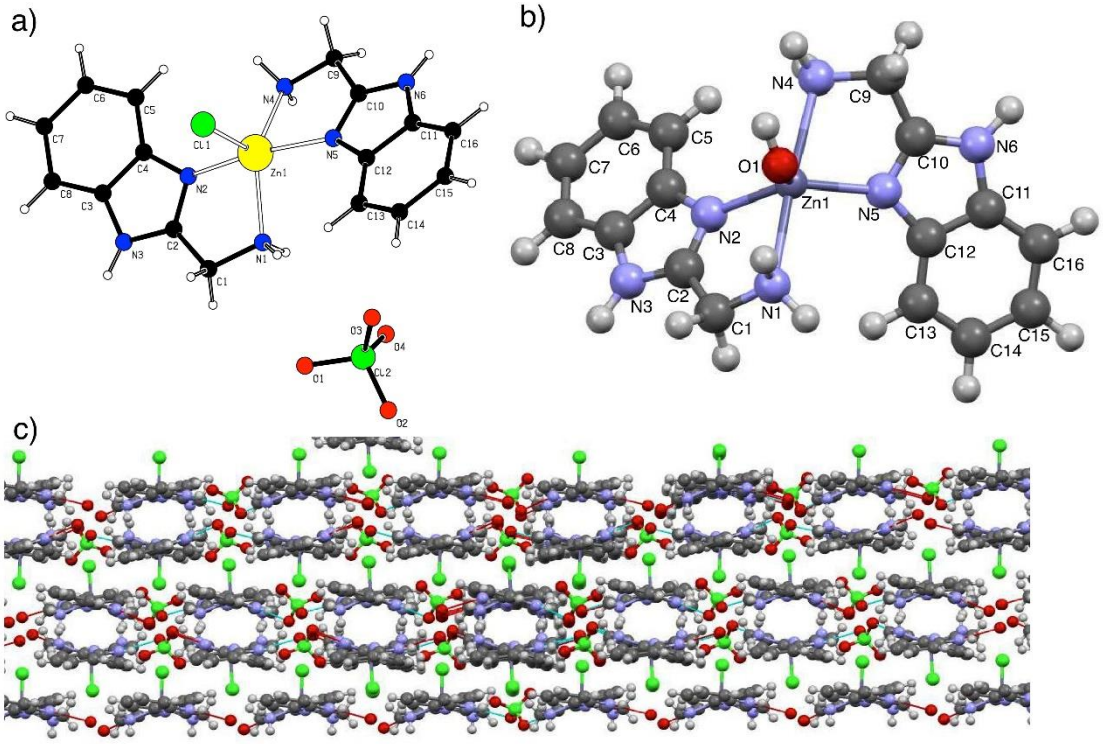

Figure 1. (**a**) ORTEP structure of complex **1**, (**b**) numbered DFT optimized structure of complex **2** and (**c**) 2D packing model of complex **1** along the a-axis showing the hydrogen bond network.

The investigated compounds behave as a 1:2 electrolyte with molar conductance values of 120 and 126 $\Omega^{-1}cm^2mole^{-1}$ for complexes **1** and **2**, respectively. This suggests that, in solution, the perchlorate ion is outside the coordination sphere. Further, the structure of zinc(II) complex **1** was also determined by using the X-ray fluorescence, in which the Zn characteristic lines (Zn-Kα at 8.632 keV and Zn-Kβ at 9.572 keV) as well as the escape peak of Zn-Kα at 6.892 keV were measured. The obtained spectrum showed that the percentage of Zn in the complex was 15.13 $\pm$ 0.21%, consistent with the elemental analysis result.

3.1.1. IR and Raman Analysis

The observed FT-IR frequencies and band assignments of the ligand AMB 2HCl and its zinc complexes **1** and **2** in the solid state are listed in Table 1. The IR spectrum of complex **1** exhibited one peak at 3326 cm^{-1} and another one at 1227 cm^{-1} assigned to hydrogen bond stretching and bending, respectively. The peak at 3388 cm^{-1} was absent in the case of the hydroxo complex **2** (Figure 2), whereas at 1227 cm^{-1}, it showed two peaks most likely due to the intramolecular hydrogen bonding in complex **1** between the hydrogen atoms of the benzene rings and coordinated chloride ligand. In complex **2**, the coordinated oxygen is blocked by hydrogen atom, which makes it not possible to form a hydrogen bond. This confirms that, in complex **1**, the extra peaks are from hydrogen bond stretching

and bending. In the solution, these extra peaks are absent. The effect of zinc(II) binding on the ring vibration of C–C–N–C in the benzimidazole ring of the ligand system was investigated. The observed bands at 1452 and 621 cm^{-1} for complex **1** were assigned as ring stretching and ring bending, respectively. These bands were shifted respectively by 18 and 25 cm^{-1} to high frequencies upon complexation with zinc(II) ions [39]. The spectra showed other bands assigned to ν(C-H) stretching, ν(C=N) and δ(C-H) bending [40].

Table 1. IR assignments of the ligand AMB·2HCl and its zinc(II) complexes **1** and **2**.

AMB·2HCl	Complex 1	Complex 2	Assignments
-	-	3588	O-H st.
3385	3326	3336	N-H/hydrogen bond st.
3230-2507 br	3259	3243	C-H/hydrogen bond st.
3039	3068	3065	C-H Benzene st.
2913	2920	2920	C1-H st.
1624, 1593	1624	1628	C=C st.
1540	1537	1538	N-H def.
1487, 1457	1494, 1475	1495, 1475	C=N st.
1442	1452	1452	C-H def.
1377, 1351	1368, 1345	1388, 1347	H-C-H ben.
1309, 1270	1315, 1279	1316, 1279	N-H Def.
1217, 1200	1227, 1213	1227, 1217	N-H roching/hydrogen bond ben.
1150, 1139	1150, 1144	1150, 1140	=C-H ben
	1064	1086	ClO_4^-
1031	1048	1048	C-N=C ben.
1018	1004	1005	C-C benzene
	752	743	ClO_4^-
621	621	626	N-H Obp.
	407	408	Zn-Cl st.
	409	412	Zn-N st.
	406	411	Zn-O st.

Additionally, the FTIR spectra of both complexes displayed weak bands at 428, 486 and 452 cm^{-1}, which suggested the existence of M–N bond. The FTIR spectrum also shows very intense absorption bands at 1064, 752 cm^{-1} and 1086, 743 cm^{-1} for zinc(II) complexes **1** and **2**, respectively. This indicates the ionic character of ClO_4^- in both complexes [41]. In the OH stretching region, a broad absorption band extending from about 3537 to 3588 cm^{-1} is detected for the coordinated hydroxide ion in complex **2**.

Information about the low frequency Zn(II)–N/O vibrations can be obtained by using Raman spectroscopy. Typical Raman spectra recorded for the ligand AMB and its Zn(II) complexes **1** and **2** are shown in Figure 3. The spectra comprised a prominent new band at 3450 cm^{-1}, resulting from the formation of Zn(II)–OH bond.

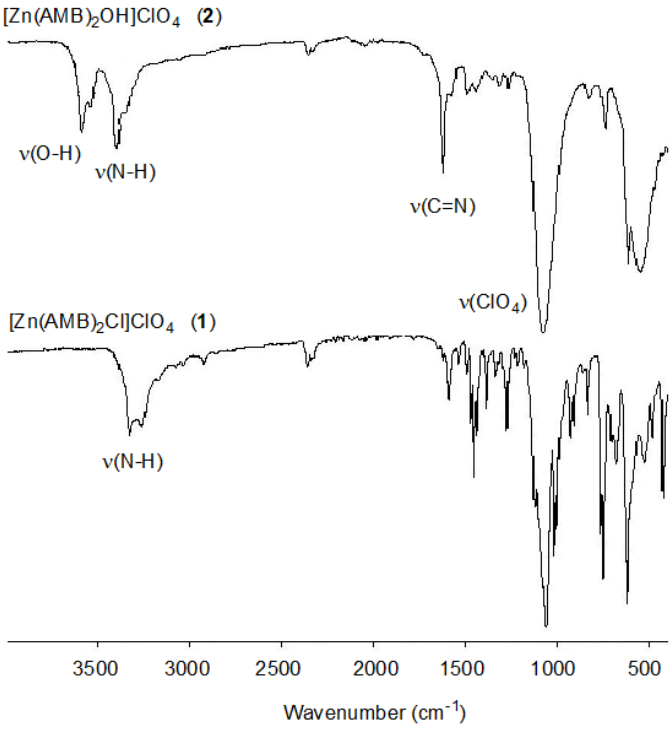

Figure 2. FTIR spectra of zinc(II) model complexes $[Zn(AMB)_2Cl](ClO_4)$ **1** and $[Zn(AMB)_2(OH)](ClO_4)$ **2**.

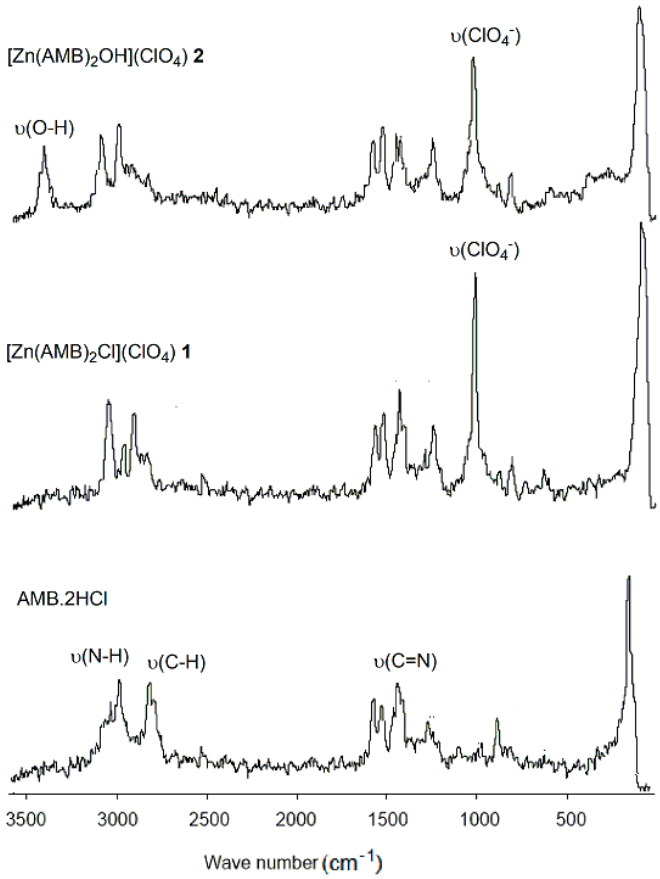

Figure 3. Raman spectra of the ligand AMB·2HCl and its zinc(II) model complexes $[Zn(AMB)_2Cl](ClO_4)$ **1** and $[Zn(AMB)_2(OH)](ClO_4)$ **2**.

3.1.2. H NMR Spectra

The stoichiometry of zinc(II) complex **1** was determined by recording the chemical shifts of the pyridine and methylene protons of the produced zinc(II) complex **1** at different ratios of solutions of the zinc salt and the ligand AMB: $R([Zn^{2+}]_0/[AMB]_0)$ = 0, 1.0, and 2.0 in CD_3OD:D_2O (3:1). In ^1H NMR spectra (Figure 4), the methylene resonances are displaced toward lower frequencies (△ = 0.42) with respect to the AMB·2HCl, which demonstrates that $H_2N \rightarrow Zn$ coordination is present in solution. Figure 4 also showed that with increasing the concentration of zinc(II) ions, there are broadening and downfield shifts of the pyridine and methylene protons of the produced zinc(II) complex species between 0 < R < 2. This finding can be attributed to the exchange interaction between the complex at the molar ratio 2:1 and the free ligand. Further increments of zinc(II) ions do not change the chemical shift, that is why the formation of zinc complexes with 2:1 stoichiometry is thought and the composition is $[Zn(AMB)_2Cl]^+$ **1**, mononuclear model complex. The ^1H NMR spectrum of the hydroxo complex $[Zn(AMB)_2(OH)]^+$ **2** showed that the methylene and pyridine nitrogen of the benzimidazole ring were upfield shifted in comparison to the chemical shift of zinc(II) complex in $[Zn(AMB)_2Cl]^+$ **1** (Figure 4) [21–24]. The 0.4–0.6 ppm downfield shift for zinc-bound OH compared with the chemical shift of free water resulted from the decrease in electron density due to the coordination to zinc(II) ion. This is mainly attributed to the effect of the Lewis acidity of zinc.

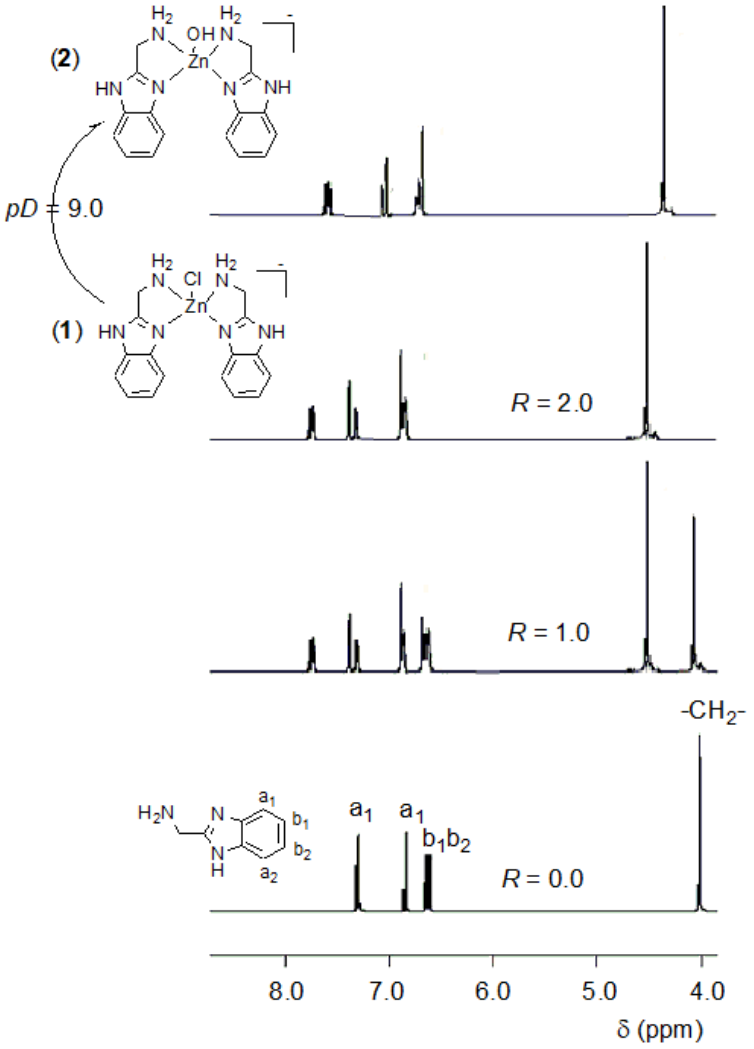

Figure 4. ^1H NMR titration of zinc(II) complex **1** (2.0×10^{-3} M) as a function of pD in CD_3OD:D_2O (3:1, I = 0.1 M $NaNO_3$, 25 ± 0.1 °C).

3.2. Cyclic Voltammetry

The electrochemical behavior of a bare carbon paste electrode (CPE), CPE modified by the AMB ligand and its Zn(II) complex **1** and **2** were studied using 5.0 mM $K_3[Fe(CN)_6]/K_4[Fe(CN)_6]$ [42] in the potential range from +1.5 to −1.5 V (vs. Ag/AgCl) at a scan rate potential of 50 mVs^{-1}. Figure 5a showed the cyclic voltammograms for a bare carbon paste electrode where no peaks were observed in the studied range. The CV of 5.0 mM of $K_3[Fe(CN)_6]/K_4[Fe(CN)_6]$ recorded on a CPE modified by AMB ligand (Figure 5b) displayed one quasi-reversible system. The oxidation peak (E_{pa}) appeared at +0.68 V and the cathodic peak (E_{pc}) appeared at −0.4 V. The separation of the anodic and cathodic peak potentials (ΔE) was found to be <1080 mV, which is corresponding to Fe(II)/Fe(III) couple. The formal potential, $E_{1/2}$ (+0.14 V), was taken as the average of both E_{pc} and E_{pa}.

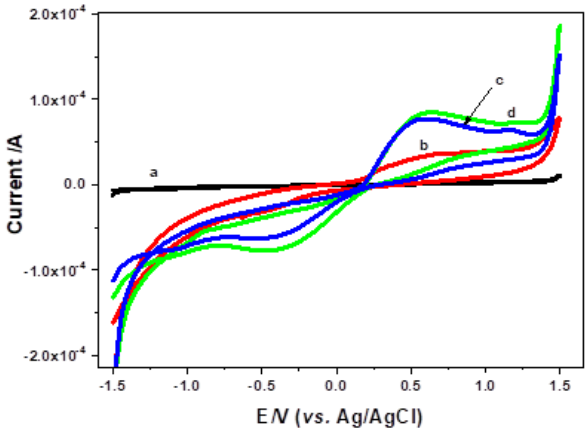

Figure 5. Cyclic voltammetric response for: (a) bare carbon paste electrode, (b) carbon paste electrode modified with AMB ligand, (c) carbon paste electrode modified with complex **1** and (d) carbon paste electrode modified with complex **2**. These used 5.0 mM $K_3[Fe(CN)_6]/K_4[Fe(CN)_6]$, a potential scan rate of 50 mV s^{-1} and a potential range from +1.5 to −1.5 V (vs. Ag/AgCl).

The CV of the CPE modified by zinc(II) complex **1** showed a well-defined quasi-reversible system (Figure 5c). The oxidation peak (E_{pa}) appeared at +0.53 V and the cathodic peak (E_{pc}) appeared at −0.38 V. The separation of the anodic and cathodic peak potentials (ΔE) was determined to be <910 mV. The formal potential $E_{1/2}$ was found to be +0.075 V. The higher peak current with zinc(II) complex **1** (Figure 5c), which is accompanied by the decrease in the peak potentials difference (ΔE_p), may be due to enhanced electrocatalytic activity of the modified electrode towards the oxidation-reduction of Fe(II)/Fe(III) ions.

Figure 5d shows the carbon paste electrode modified with Zn complex **2**. A well-defined one quasi-reversible system, the oxidation peak (Epa1) appeared at +0.53 V and the cathodic peak (E_{pc1}) appeared at −0.38 V. The separation of the anodic and cathodic peak potentials (ΔE) was found to be <910 mV, corresponding to the Fe(II)/Fe(III) couple. The formal potential $E_{1/2}$ was taken as the average of E_{pc1} and Epa1, and is +0.075 V.

As shown in Figure 5, the peak currents obtained at a carbon paste electrode modified with complex **1** and **2** were much larger than that for a bare carbon paste electrode modified by AMB ligand. Additionally, the peak current at a carbon paste electrode modified with complex **2** was much larger than that for a bare carbon paste electrode modified by complex **1**. This may be due to that the catalytic activity was increased by the addition of complex **1** and **2**. This was observed from the large increase in the peak current especially in case carbon paste modified by complex **2** and the decrease in the difference between peak potentials (ΔE_p). This may be due to that the catalytic activity of **2** was higher than **1**, which is attributed to the higher electronegativity of **2** due to the hydroxyl group. So, carbon paste modified by complex **2** was selected for further work.

3.3. Electrochemical Impedance Spectroscopic Study

To obtain detailed information about the electrode/solution interface, the electrical equivalent circuit from the CPE modified by zinc(II) complex **1** and **2** in the absence and presence of $[Fe(CN)_6]^{3-/4-}$ as an electrochemical redox system compatible is shown in Figure 6a. This system comprises a solution/electrolyte resistance (R_s), a constant phase element (Q), corresponding to the double layer capacitance, and a charge transfer resistance (R_{ct}) associated with the oxidation of low valence mediator species. Figure 6b represents the Nyquist diagrams of the bare CPE and the CPE modified with the AMB ligand and Zn(II) complex **1** and **2** in a solution containing 5.0 mM of $[Fe(CN)_6]^{3-/4-}$ and 1.0 M of KCl. The Nyquist plot is a semicircle domain with R_{ct} of ~312.735, 19.725, 14.65 and 12.540 KΩ cm^2 for the bare CPE, CPE modified with ligand AMB, zinc(II) complex **1** and complex **2**, respectively. This result showed that, upon addition of the ligand AMB, zinc(II) complex **1** and **2** to CPE, the shape of Nyquist plot is decreased in comparison to bare CPE. The polarization resistance for the three electrodes was increased in the sequence of bare CPE > CPE modified by the ligand AMB > CPE modified by the zinc(II) complex **1** > complex **2**. The lower value of R_{ct} at the surface of CPE modified by Zn(II) complex **2** indicates that Zn(II) complex **2** can promote the electron transfer and accordingly accelerates the diffusion of ferricyanide towards the electrode surface, which improves the conductivity. In addition, complex **2** showed a lower R_{ct} value than **1**, which indicates that the former is more active. So, the conductivity was improved by the modification of CPE by Zn (II) complex **2**.

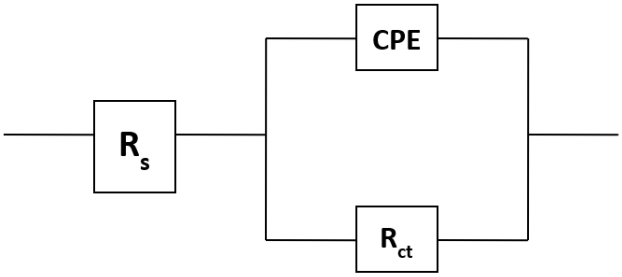

(**A**)

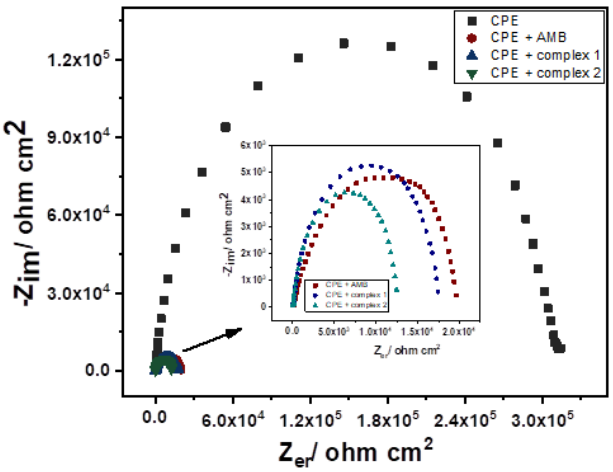

(**B**)

Figure 6. Equivalent circuit (**A**) and Nyquist plots (**B**) of bare CPE (a), CPE modified by AMB (b), CPE modified by Zn complex 1 (c) and CPE modified by Zn complex 2 (d) in a solution containing 1 mM $[Fe(CN)_6]^{3-/4-}$ and 5 M KCl.

3.4. Amperometric Determination of Organophosphorus Compounds

The amperometric determination of OPs compounds by the anodic oxidation of the enzymatically produced *p*-nitrophenol is reported [43–47]. Figure 7 exhibits the cyclic voltammograms of 1.0 mM *p*-nitrophenol on CPE modified with Zn(II) complex **2** in phosphate buffer at different pH values ranging from 7.0 to 10.0. The results showed that the *p*-nitrophenol has an anodic oxidation peak over the range from +1.0 V to 0.97 V (vs. Ag/AgCl) at all the different pH values studied, except at pH = 8.0, where an additional oxidation peak appeared at +0.2 V. The peak current height increased by increasing pH value from 7.0 to 8.0; after that, the oxidation peak current decreased (Figure 6). So, phosphate buffer (pH 8) was selected for the detection of the produced *p*-nitrophenol form the decomposition of OPs.

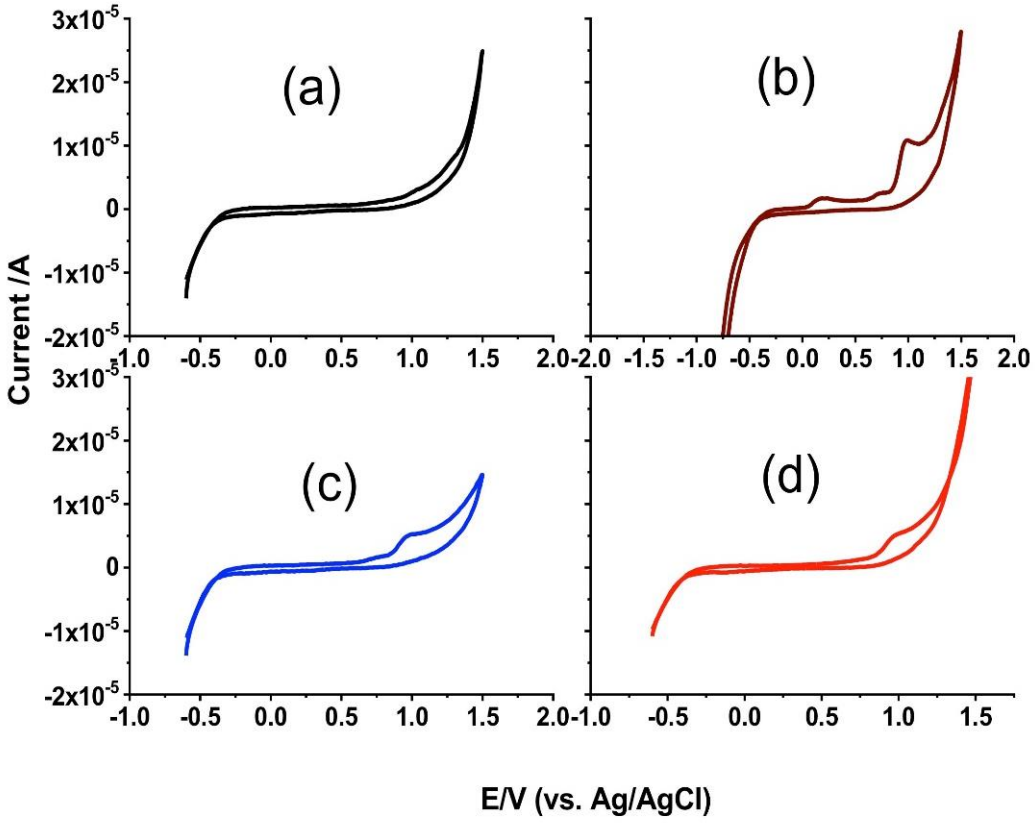

Figure 7. Cyclic voltammograms of 1.0 mM of *p*-nitrophenol at a CPE modified with Zn(II) complex **2** at different pH values: (**a**) 7, (**b**) 8, (**c**) 9 and (**d**) 10; scan rate = 50 mV/s.

The electrochemical behavior of the toxic OPs, fenitrothion and parathion (1×10^{-3} M), was examined on CPE modified by Zn(II) complex **2** in the presence of CTAB (1×10^{-3} M) in the potential range from −1.0 to +1.5 V (vs. SCE). The results showed that parathion gave only one oxidation peak at +0.8 V and no reduction peaks appeared in the reverse scan (Figure 8), whereas fenitrothion exhibited an irreversible oxidation peak at ~0.88 V (vs. Ag/AgCl) (Figure 8b).

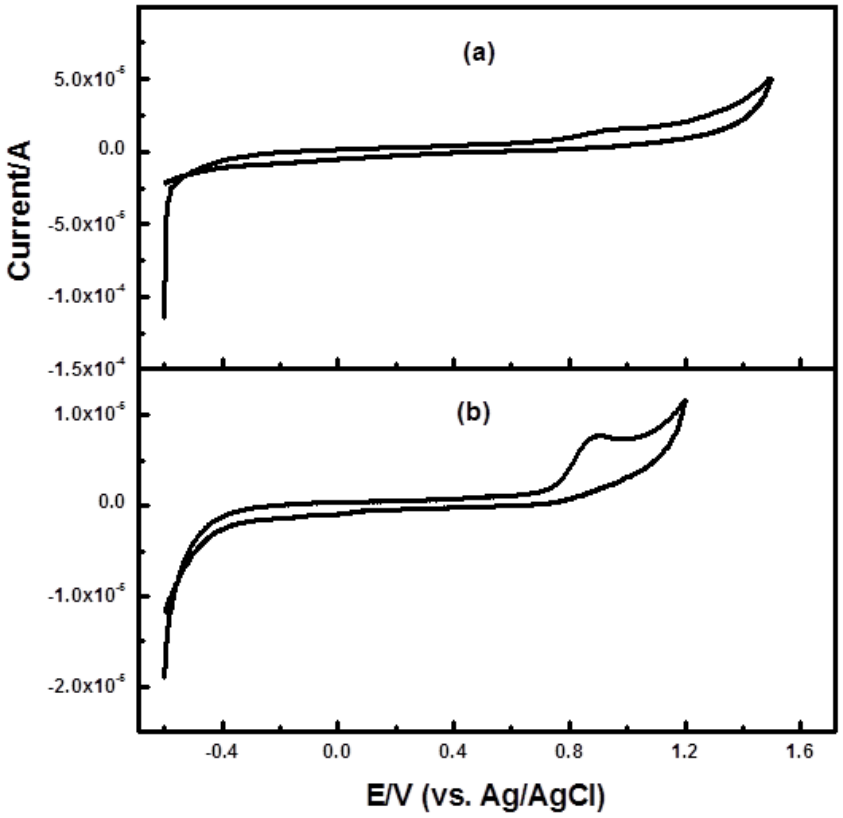

Figure 8. Electrochemical behavior of 1×10^{-3} M (**a**) parathion and (**b**) fenitrothion in a phosphate buffer (pH = 8.0) using cyclic voltammetry.

The above-mentioned electrochemical behaviors of parathion and fenitrothion at CPE modified by Zn(II) complex **2** showed one anodic oxidation peak at ~0.88 V (vs. Ag/AgCl). This peak was also observed at the same position for the oxidation of *p*-nitrophenol [48]. This indicates that the CPE modified by Zn(II) complex **2** acts as a **biomimetic hydrolase enzyme** sensor for the determination of OPs, in which fenitrothion and parathion hydrolyze to generate *p*-nitrophenol (Scheme 1), which is oxidized at the surface of CPE.

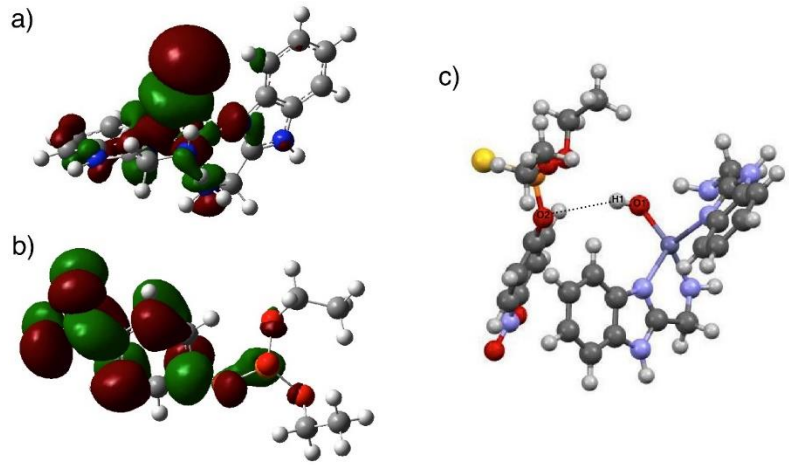

Scheme 1. (**a**) Calculated (DFT) HOMO orbital of the complex **2**, (**b**) calculated (DFT) LUMO orbital of the substrate (Parathion) and (**c**) the calculated (DFT) **2**. OPs complex stabilized by hydrogen bond.

3.5. Stability of Carbon Paste Modified Electrode Modified by Complex **2**

To examine the stability of the prepared biomimetic sensor, ten repetitive cyclic voltammograms of both parathion and fenitrothion (1×10^{-3} M) in phosphate buffer (pH 8) in

presence of CTAB (1×10^{-3} M) were recorded. The peak current of fenitrothion decreased by repeating the cyclic voltammograms from cycle 1 to 10 (Figure 9).

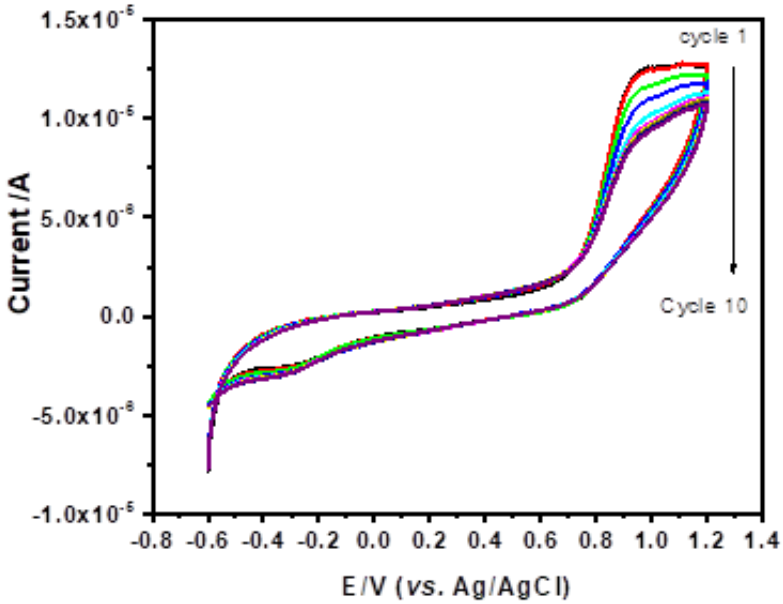

Figure 9. The repetitive cyclic voltammograms for 1×10^{-3} M fenitrothion in phosphate buffer (pH 8) in presence of CTAB (1×10^{-3} M).

3.6. Effect of Scan Rate

The effect of scan rate on the peak current of fenitrothion was studied in phosphate buffer (pH 8) in presence of CTAB (1×10^{-3} M) from 10 mV/s to 100 mV/s. By increasing scan rate values, the anodic and cathodic peak current increased (Figure 10).

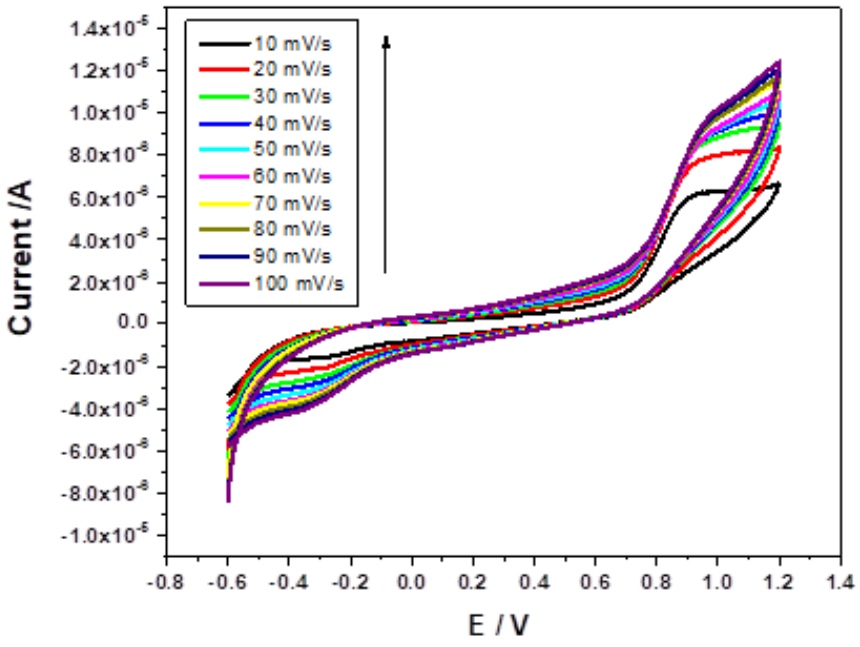

Figure 10. Effect of scan rate (from 10 to 100 mV/s) on the cyclic voltammograms for 1×10^{-3} M fenitrothion in phosphate borate buffer pH 8 in presence of CTAB with 50 mV/s scan rate.

3.7. Square Wave Voltammetric Determination of Fenitrothion and Parathion

The obtained square wave voltammograms of parathion and fenitrothion at a CPE modified by Zn(II) complex **2** using phosphate buffer (pH = 8.0) in presence of CTAB

(1.0×10^{-3} M) revealed a well-defined oxidation peak current at +0.89 V (vs. Ag/AgCl). Upon increasing parathion and fenitrothion concentration, the peak current signal increased. The effect of different concentrations of fenitrothion 0.1 μM (0.29 ppm) to 5.5 μM (0.1.6 ppm) on the peak current was examined (Figure 11a). The obtained calibration curve (Figure 11b) showed a linear behavior with a correlation coefficient of 0.996 and a relative standard deviation (RSD) of 2.253×10^{-7}. In addition, the effect of different concentrations of parathion 0.1 μM (0.028 ppm) to 1.0 μM (0.28 ppm) on the peak current was investigated (Figure 11c). A straight line was obtained with a correlation coefficient of 0.997 and a relative standard deviation (RSD) of 2.58×10^{-7}. The lower detection limits of 0.51 μM (0.149 ppm) and 0.08 μM (0.022 ppm) were calculated for parathion and fenitrothion, respectively, based on the formula LOD = 3(SD/m).

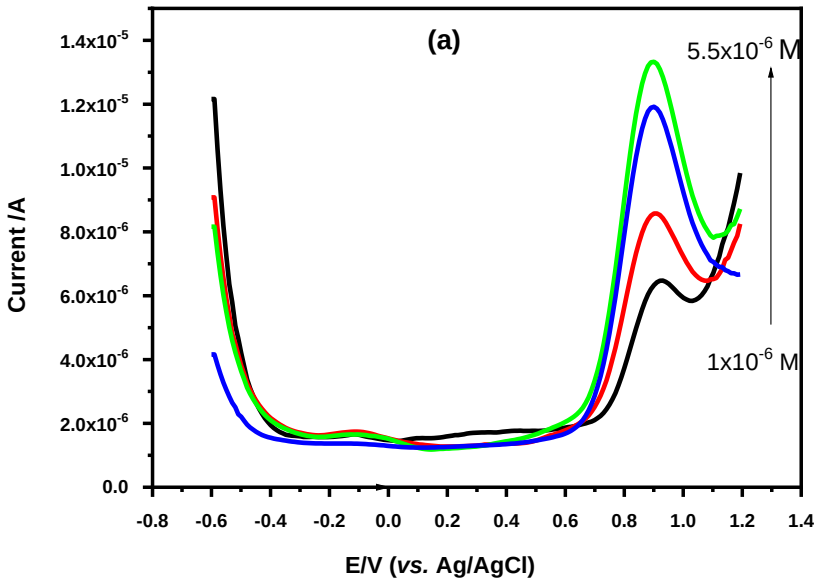

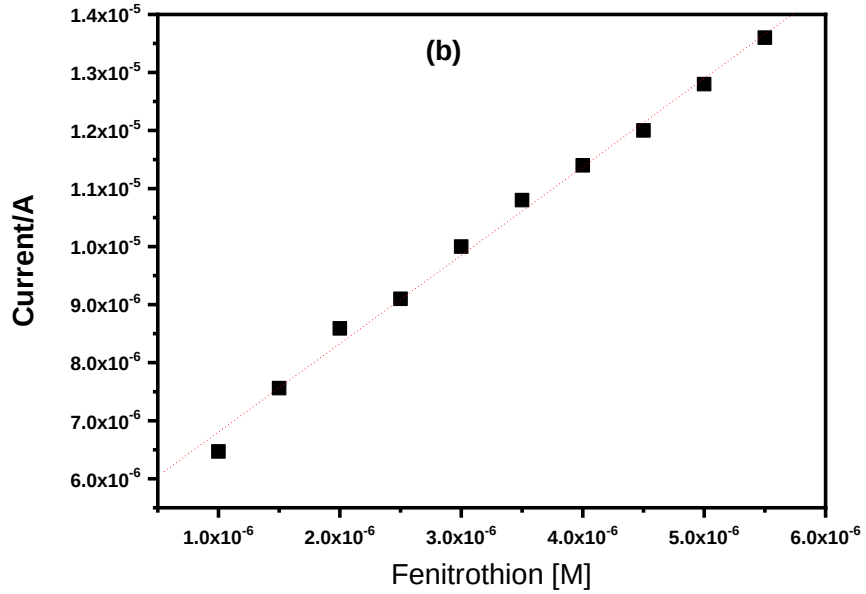

Figure 11. *Cont.*

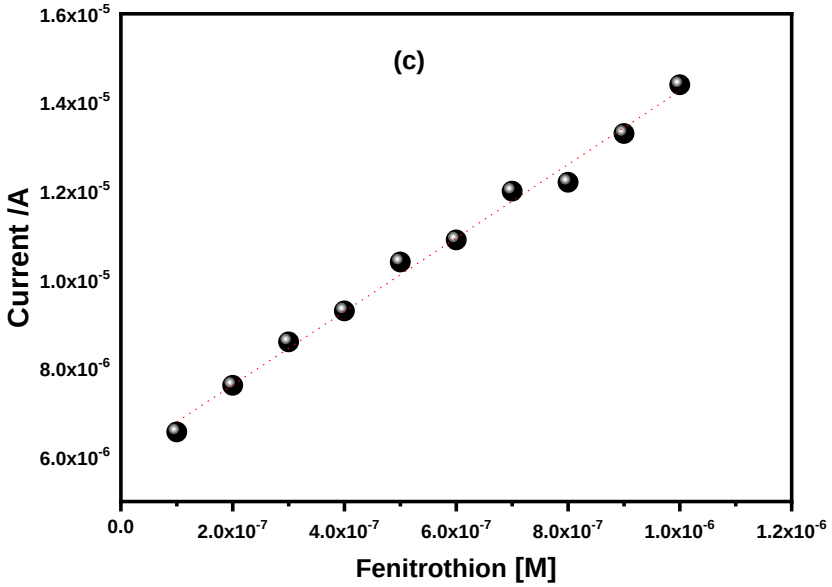

Figure 11. Effect of different concentration in the square wave voltammetric voltammograms on the peak current signal for fenitrothion (**a**), calibration plot for fenitrothion (**b**) and calibration plot for parathion (**c**) in a phosphate buffer (pH = 8.0) using cyclic voltammetry.

The above-mentioned analytical results showed that the modification of CPE by Zn(II) complex **1** improved its electrocatalytic activity, while complex **2** considerably increased the activity more than complex **1**. This may be ascribed to the higher electronegativity of hydroxyl group in **2** than Cl in **1**. These obtained artificial biomimetic sensor for the hydrolysis and detection of OPs.

On the basis of the electrochemical properties of both **1** and **2** towards the hydrolysis of OPs (fenitrothion and parathion) and the DFT calculations, we proposed a mechanism for the hydrolysis of fenitrothion and parathion (Scheme 1). Complex **1** has a dominant structure at lower pH values with the Cl atom coordinated to the the Zn atom, while at high pH, Cl was replaced by hydroxyl group (complex **2**). Then, the zinc center delivers the coordinated hydroxyl, which can nucleophilically attack the parathion molecule. TD-DFT calculation of **2** reveals that the HOMO orbitals (electron density) (Scheme 1a) are situated on the Zn-OH center, which is the active center, while the LUMO center of the substrate (parathion) (Scheme 1b) is situated on the *p*-nitrophenolate, which is active to receive the electron from **2**. The process initiated by the hydrogen bond formation between the hydroxyl group and the O atom at the *p*-nitrophenolate moiety is presented in Scheme 1c.

Simultaneously, the zinc ion withdraws electron density away from the phosphorus atom, forming a penta-coordinated intermediate (Scheme 2). Finally, the *p*-nitrophenolate is released and the zinc(II)-bound diethyl thiophosphate, which could be isolated from the solvent and replaced by water to form again the starting catalyst aqua zinc(II) complex, which is ready to start another catalytic cycle.

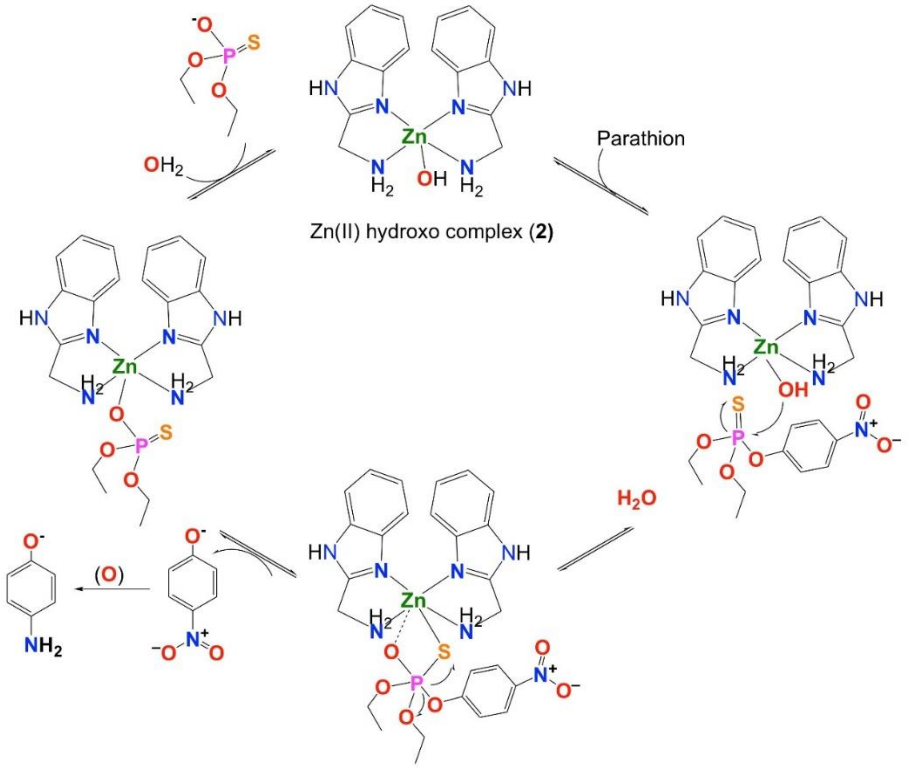

Scheme 2. Proposed mechanism for the hydrolysis of parathion with complex **2**.

4. Conclusions

A chlorobis(2-aminomethylbenzimidazole)zinc(II) perchlorate complex $[Zn(AMB)_2Cl](ClO_4)$ **1** and its hydroxo species $[Zn(AMB)_2(OH)](ClO_4)$ **2** as a functional mimic for the active site of **organophosphorus hydrolase enzyme** were used for the construction of a biomimetic sensor for the determination of the toxic organophosphorus OPs fenitrothion and parathion by square wave voltammetry. The electrochemical behavior of these toxic OPs was studied at the bare CPE and at the surface of CPE modified by Zn(II) complex **1** and **2**. Modification of CPE by Zn(II) complex **1** increased the electrocatalytic activity of this electrode, while the addition of complex **2** significantly increases the activity, which attributed to the higher electronegativity of hydroxyl group than Cl. The prepared biomimetic sensor provides a microenvironment for the simultaneous hydrolysis and detection of OPs.

Author Contributions: Conceptualization, G.A.M.M. and M.M.I.; methodology, M.M.I.; software, H.S.E.-S.; validation, M.A.A., N.Y.M. and R.B.; formal analysis, G.A.M.M.; investigation, M.M.I.; resources, G.A.M.M.; data curation, N.Y.M.; writing—original draft preparation, A.M.; writing—review and editing, A.M.; visualization, G.A.M.M.; supervision, G.A.M.M.; project administration, G.A.M.M. development of methodology; creation of models, S.A. All authors have read and agreed to the published version of the manuscript.

Funding: Taif University: KSA, Project Number: 1/440/6172.

Institutional Review Board Statement: No Board Statement.

Informed Consent Statement: No Consent Statement.

Data Availability Statement: No Data Availability.

Acknowledgments: This work was financially supported by the High Attitude Research Center, Taif University, KSA Project Number: 1/440/6172.

Conflicts of Interest: The authors declare that they have no conflict of interests.

References

1. Mersal, G.A.M.; Ibrahim, M.M. Solution studiesof tris(2-benzylaminoethyl)amine complexes of zinc(II) and copper(II): The catalytic hydrolysis of toxic organophosphate. *Comptes Rendus Chim.* **2012**, *15*, 336–345. [CrossRef]
2. Ibrahim, M.M.; Ramadan, A.M. Thioimidazolate versuspyrazolate-zinc(II)-bound hydroxo complex as structural model for the active site of hydrolytic enzyme: The crystal structure of the inclusion complex TtZn–O–C_6H_4–p-NO_2, Tt 5 hydrotris(N-xylyl-2-thioimidazolyl)borate. *J. Incl. Phenom. Macrocycl. Chem.* **2012**, *72*, 103–111. [CrossRef]
3. Ibrahim, M.M. Synthesis andspectroscopic characterization of zinc(II) and copper(II) complexes of N,N-bis(2-picolyl)glycine as structural phosphotriestrase models: The catalyzed detoxification of paraoxon. *J. Mol. Struct.* **2011**, *990*, 227–236. [CrossRef]
4. Ibrahim, M.M.; Shimomura, N.; Ichikawa, K.; Shiro, M. Phosphoester hydrolysisusing structural phosphatase models of tren based zinc(II) complexes and X-ray crystal structures of [Zn(tren)(H_2O)](ClO_4)$_2$ and [Zn(tren)(BNPP)]ClO_4. *Inorg. Chim. Acta* **2001**, *313*, 125–136. [CrossRef]
5. Čolović, M.B.; Krstić, D.Z.; Lazarević-Pašti, T.D.; Bondžić, A.M.; Vasić, V.M. Acetylcholinesterase Inhibitors: Pharmacology and Toxicology. *Curr. Neuropharmacol.* **2013**, *11*, 315–335. [CrossRef]
6. Serdar, C.M.; Gibson, D.T. Enzymatic Hydrolysisof Organophosphates: Cloning and Expression of a Parathion Hydrolase Gene from *Pseudomonas diminuta*. *Bio/Technology* **1985**, *3*, 567–575.
7. Yan, X.; Shi, H.; Wang, M. Development ofan enzyme-linked immunosorbent assay for the simultaneous determination of parathion and imidacloprid. *Anal. Methods* **2012**, *4*, 4053–4057. [CrossRef]
8. Mehta, J.; Dhaka, S.; Bhardwaj, N.; Paul, A.K.; Dayananda, S.; Lee, S.-E.; Kim, K.-H.; Deep, A. Application ofan enzyme encapsulated metal-organic framework composite for convenient sensing and degradation of methyl parathion. *Sens. Actuators B Chem.* **2019**, *290*, 267–274. [CrossRef]
9. Kucherenko, I.S.; Soldatkin, O.O.; Dzyadevych, S.V.; Soldatkin, A.P. Electrochemical biosensorsbased on multienzyme systems: Main groups, advantages and limitations—A review. *Anal. Chim. Acta* **2020**, *1111*, 114–131. [CrossRef] [PubMed]
10. Vincent, A.; Fores, J.R.; Tauziet, E.; Quévrain, E.; Dancs, Á.; Conte-Daban, A.; Bernard, A.-S.; Pelupessy, P.; Coulibaly, K.; Seksik, P.; et al. An easy-to-implement combinatorial approach involving an activity-based assay for the discovery of a peptidyl copper complex mimicking superoxide dismutase. *Chem. Commun.* **2020**, *56*, 399–402. [CrossRef]
11. Biniuri, Y.; Shpilt, Z.; Albada, B.; Vázquez-González, M.; Wolff, M.; Hazan, C.; Golub, E.; Gelman, D.; Willner, I. A Bis-Zn^{2+}-Pyridyl-Salen-Type Complex Conjugated to the ATP Aptamer: An ATPase-Mimicking Nucleoapzyme. *ChemBioChem* **2020**, *21*, 53–58. [CrossRef]
12. Salonen, P.; Peuronen, A.; Lehtonen, A. Bioinspired Mo, W and V complexes bearing a highly hydroxyl-functionalized Schiff base ligand. *Inorg. Chim. Acta* **2020**, *503*, 119414–119429. [CrossRef]
13. Gavrllova, A.L.; Bosnich, B. Principles ofMononucleating and Binucleating Ligand Design. *Chem. Rev.* **2004**, *104*, 349–383. [CrossRef] [PubMed]
14. Ibers, J.A.; Holm, R.H. Modeling coordinationsites in metallobiomolecules. *Science* **1980**, *209*, 223–235. [CrossRef] [PubMed]
15. Karlin, K.D. Metalloenzymes, structural motifs, and inorganic models. *Science* **1993**, *261*, 701–708. [CrossRef] [PubMed]
16. Parkin, G. The bioinorganicchemistry of zinc: Synthetic analogues of zinc enzymes that feature tripodal ligands. *Chem. Commun.* **2000**, *20*, 1971–1985. [CrossRef]
17. Ibrahim, M.M.; Ramadan, A.M.; Mersal, G.A.M.; El-Shazly, S.A. Synthesis, Characterization, and Electrochemical Properties of Bis(2-benzimidazolylmethyl- 6-sulfonate) amine-based zinc(II), copper(II), and oxidovanadium(IV) Complexes: SOD. Scavenging, DNA binding, and Anticancer Activities. *Int. J. Electrochem. Sci.* **2012**, *7*, 7526–7546.
18. Ibrahim, M.M.; Amin, M.A.; Ichikawa, K. Synthesis andcharacterization of benzimidazole-based zinc complexes as structural carbonic anhydrase models and their applications towards CO_2 hydration. *J. Mol. Struct.* **2011**, *985*, 191–201. [CrossRef]
19. Echizen, T.; Ibrahim, M.M.; Nakata, K.; Izumi, M.; Ichikawa, K.; Shiro, M. Nucleophilic reactionby carbonic anhydrase model zinc compound: Characterization of intermediates for CO_2 hydration and phosphoester hydrolysis. *J. Inorg. Biochem.* **2004**, *98*, 1347–1360. [CrossRef]
20. Valencia, T.M.G.; de Llasera, M.P.G. Determination of organophosphorus pesticides in bovine tissue by an . . . extraction–high performance liquid chromatography with diode array detection method. *J. Chromatogr. A* **2011**, *1218*, 6869–6877. [CrossRef]
21. Yang, T.; Lee, M. Electrically assistedsolid-phase microextraction combined with liquid chromatography–mass spectrometry for determination of parathion in water. *Talanta* **2010**, *82*, 766–770. [CrossRef] [PubMed]
22. Nousiainen, M.; Peräkorpi, K.; Sillanpää, M. Determination ofGas-Phase Produced Ethyl Parathion and Toluene 2,4-diisocyanate by Ion Mobility Spectrometry, Gas Chromatography and Liquid Chromatography. *Talanta* **2007**, *72*, 984–990. [CrossRef]
23. Kumaravel, A.; Chandrasekaran, M. A novelnanosilver/nafion composite electrode for electrochemical sensing of methyl parathion and parathion. *J. Electroanal. Chem.* **2010**, *638*, 231–235. [CrossRef]
24. Sanghavi, B.J.; Hirsch, G.; Karna, S.P.; Srivastava, A.K. Potentiometric StrippingAnalysis of Methyl and Ethyl Parathion Employing Carbon Nanoparticles and Halloysite Nanoclay Modified Carbon Paste Electrode. *Anal. Chim. Acta* **2012**, *735*, 37–45. [CrossRef]
25. Dzyadevych, S.V.; Soldatkin, A.P.; Arkhypova, V.N.; El'skaya, A.V.; Chovelon, J.; Georgiou, C.A.; Martelet, C.; Jaffrezic-Renault, N. Early-warning electrochemical biosensor system for environmental monitoring based on enzyme inhibition. *Sens. Actuators B* **2005**, *105*, 81–87. [CrossRef]
26. Zhou, Q.; Yang, L.; Wang, G.; Yang, Y. Acetylcholinesterase biosensorbased on SnO_2 nanoparticles–carboxylic graphene–nafion modified electrode for detection of pesticides. *Biosens. Bioelectron.* **2013**, *49*, 25–31. [CrossRef]

27. Raghu, P.; Kumara Swamy, B.E.; Madhusudana Reddy, T.; Chandrashekar, B.N.; Reddaiah, K. Sol–gel immobilized biosensor for the detection of organophosphorous pesticides: A voltammetric method. *Bioelectrochemistry* **2012**, *83*, 19–24. [CrossRef]
28. Raghu, P.; Madhusudana Reddy, T.; Kumara Swamy, B.E.; Chandrashekar, B.N.; Reddaiah, K.; Sreedhar, M. Development ofAChE biosensor for the determination of methyl parathion and monocrotophos in water and fruit samples: A cyclic voltammetric study. *J. Electroanal. Chem.* **2012**, *665*, 76–82. [CrossRef]
29. Tian, X.; Liu, L.; Li, Y.; Yang, C.; Zhou, Z.; Nie, Y.; Wang, Y. Nonenzymatic electrochemicalsensor based on CuO-TiO_2 for sensitive and selective detection of methyl parathion pesticide in ground water. *Sens. Actuators B Chem.* **2018**, *256*, 135–142. [CrossRef]
30. Govindasamy, M.; Mani, V.; Chen, S.-M.; Chen, T.-W.; Sundramoorthy, A.K. Methyl parathiondetection in vegetables and fruits using silver@graphene nanoribbons nanocomposite modified screen printed electrode. *Sci. Rep.* **2017**, *7*, 46471. [CrossRef] [PubMed]
31. Wu, B.; Hou, L.; Du, M.; Zhang, T.; Wang, Z.; Xue, Z.; Lu, X. A molecularlyimprinted electrochemical enzymeless sensor based on functionalized gold nanoparticle decorated carbon nanotubes for methyl-parathion detection. *RSC Adv.* **2014**, *4*, 53701–53710. [CrossRef]
32. Wang, M.; Li, Z. Nano-composite ZrO_2/Au film electrode for voltammetric detection of parathion. *Sens. Actuators B Chem.* **2008**, *133*, 607–612. [CrossRef]
33. Manavalan, S.; Veerakumar, P.; Chen, S.-M.; Lin, K.-C. Three-dimensional zinc oxide nanostars anchored on graphene oxide for voltammetric determination of methyl parathion. *Microchim. Acta* **2019**, *187*, 17. [CrossRef] [PubMed]
34. Yuan, J.; Jiang, L.; Tan, X.; Yue, Y.; Shi, H.; Feng, S. Fabrication ofZr (IV) Modified Gold Electrode via Layer-by-Layer Self-Assembly for Methyl Parathion. *J. Electrochem. Soc.* **2020**, *167*, 027519. [CrossRef]
35. Ravi, A.K.; Punnakkal, N.; Punathil Vasu, S.; Nair, B.G.; T.G., S.B. Manganese dioxide based electrochemical sensor for the detection of nitro-group containing organophosphates in vegetables and drinking water samples. *J. Electroanal. Chem.* **2020**, *859*, 113841. [CrossRef]
36. Amin, M.A.; Ibrahim, M.M.; Gobouri, A.A.; Mersal, G.A.M.; Mostafa, N.Y.; Altalhi, T.; Al-Juaid, S. A newly synthesized single crystal zinc complex as molecular electrocatalyst for efficient hydrogen generation from neutral aqueous solutions. *Int. J. Hydrog. Energy* **2017**, *41*, 25980–25995. [CrossRef]
37. Frisch, M.J.; Trucks, G.W.; Schlegel, H.B.; Scuseria, G.E.; Robb, M.A.; Cheeseman, J.R.; Scalmani, G.; Barone, V.; Mennucci, B. (Eds.) *Gaussian 09*; Revision A.2; G.A.E.A. Petersson: Wallingford, CT, USA, 2009.
38. Wu, H.-Y.; Li, H.; Zhu, B.-L.; Wang, S.-R.; Zhang, S.-M.; Wu, S.-H.; Huang, W.-P. The synthesisand crystal structures of new 2-aminomethylbenzimidazole Zinc(II) complexes exhibiting luminescence. *Transit. Metal. Chem.* **2008**, *33*, 9–15. [CrossRef]
39. Ibrahim, M.M.; Ramadan, A.-M.M.; El-Sheshtawy, H.S.; Mohamed, M.A.; Soliman, M.; Zayed, S.I.M. Synthesis, characterization and medical efficacy (hepatoprotective and antioxidative) of albendazole-based copper(II) complexes—an experimental and theoretical approach. *J. Coord. Chem.* **2015**, *68*, 4296–4313. [CrossRef]
40. El-Sheshtawy, H.S.; Ibrahim, M.M.; Aly, M.R.E.; El-Kemary, M. Spectroscopic and structure investigation of the molecular complexes of tris(2-aminoethyl)amine with π-acceptors. *J. Mol. Liq.* **2016**, *213*, 82–91. [CrossRef]
41. Ibrahim, M.M.; El-Sheshtawy, H.S.; El-Kemary, M.; Al-Juaid, S.; Youssef, M.; El-Azab, I.H. Synthesis, structure characterization, and anticancer activity of a novel oxygen-bridged tricyclic Biginelli adduct. *J. Mol. Struct.* **2017**, *1137*, 714–719. [CrossRef]
42. Moradi, R.; Sebt, S.A.; Karimi-Maleh, H.; Sadeghi, R.; Karimi, F.; Bahari, A.; Arabi, H. Synthesis andapplication of FePt/CNTs nanocomposite as a sensor and novel amide ligand as a mediator for simultaneous determination of glutathione, nicotinamide adenine dinucleotide and tryptophan. *Phys. Chem. Chem. Phys.* **2013**, *15*, 5888–5897. [CrossRef]
43. Gonçalves-Filho, D.; Silva, C.C.G.; De Souza, D. Pesticides determination in foods and natural waters using solid amalgam-based electrodes: Challenges and trends. *Talanta* **2020**, *212*, 120756. [CrossRef] [PubMed]
44. Renganathan, V.; Balaji, R.; Chen, S.-M.; Kokulnathan, T. Coherent designof palladium nanostructures adorned on the boron nitride heterojunctions for the unparalleled electrochemical determination of fatal organophosphorus pesticides. *Sens. Actuators B Chem.* **2020**, *307*, 127586. [CrossRef]
45. Lei, Y.; Mulchandani, P.; Wang, J.; Chen, W.; Mulchandani, A. Highly Sensitiveand Selective Amperometric Microbial Biosensor for Direct Determination of p-Nitrophenyl-Substituted Organophosphate Nerve Agents. *Environ. Sci. Technol.* **2005**, *39*, 8853–8857. [CrossRef]
46. Mersal, G.A.M.; Ibrahim, M.M.; Fadllalh, S.; El-Sheshtawy, H.S.; Al-Malki, M.M. The Electrocatalytic Activity of Pyrazolyl-thioimidazolyl boratebased Zinc(II) Complexes Towards the Hydrolysis of Tris(pnitrophenyl)phosphate. *Int. J. Electrochem. Sci.* **2017**, *12*, 710–725. [CrossRef]
47. Hossain, M.M.; Faisal, S.N.; Kim, C.S.; Cha, H.J.; Nam, S.C.; Lee, H.J. Amperometric protonselective strip-sensors with a microelliptic liquid/gel interface for organophosphate neurotoxins. *Electrochem. Commun.* **2011**, *13*, 611–614. [CrossRef]
48. Arvinte, A.; Mahosenaho, M.; Pinteala, M.; Sesay, A.; Virtanen, V. Electrochemical oxidationof p-nitrophenol using graphene-modified electrodes, and a comparison to the performance of MWNT-based electrodes. *Microchim. Acta* **2011**, *174*, 337–343. [CrossRef]